Clim Dyn
DOI 10.1007/s00382-011-1111-4

Mixed layer heat budget of the El Niño in NCEP climate forecast system

Boyin Huang · Yan Xue · Hui Wang · Wanqiu Wang · Arun Kumar

Received: 10 March 2011 / Accepted: 25 May 2011

Abstract The mechanisms controlling the El Niño have been studied by analyzing mixed layer heat budget of daily outputs from a free coupled simulation with the Climate Forecast System (CFS). The CFS is operational at National Centers for Environmental Prediction, and is used by Climate Prediction Center for seasonal-to-interannual prediction, particularly for the prediction of the El Niño and Southern Oscillation (ENSO) in the tropical Pacific. Our analysis shows that the development and decay of El Niño can be attributed to ocean advection in which all three components contribute. Temperature advection associated with anomalous zonal current and mean vertical upwelling contributes to the El Niño during its entire evolutionary cycle in accordance with many observational, theoretical, and modeling studies. The impact of anomalous vertical current is found to be comparable to that of mean upwelling. Temperature advection associated with mean (anomalous) meridional current in the CFS also contributes to the El Niño cycle due to strong meridional gradient of anomalous (mean) temperature. The surface heat flux, non-linearity of temperature advection, and eddies associated with tropical instabilities waves (TIW) have the tendency to damp the El Niño. Possible degradation in the analysis and closure of the heat budget based on the monthly mean (instead of daily) data is also quantified.

1 Introduction

The El Niño and Southern Oscillation (ENSO) is the dominant tropical mode of climate variability associated with sea surface temperature (SST), precipitation and winds, and has a time scales of 3–7 years (Philander 1990). Numerous observations and model simulations showed that the ENSO has profound impacts on the global climate (Webster et al. 1998) including temperature and precipitation (Yulaeva and Wallace 1994), Eurasian snow cover (Barnett et al. 1988), East Asian monsoon (Wang et al. 2000), US drought (Ropelewski and Halpert 1986), and Atlantic hurricane and western Pacific Typhoon (Gray 1984). ENSO can also affect various global modes of climate variability such as Pacific Decadal Oscillation (PDO; e.g. Newman et al. 2003), North Atlantic Oscillation (NAO; e.g. Mokhov and Smirnov 2006), Tropical Atlantic Variability (Hu and Huang 2007), and Indian Ocean Dipole (IOD; Behera et al. 2006). Further, studies have also shown that ENSO carries the most significant signal in the climate predictability (Latif et al. 1998) not only in the tropical Pacific (Jin et al. 2008) but also in the North Pacific (Alexander et al. 2008) and tropical Atlantic (Chang et al. 2003).

Extensive studies during the past several decades have focused on understanding the mechanisms of ENSO, which is believed to result from the coupling between the ocean and atmosphere (Bjerknes 1969; Wrytki 1975; Zebiak and Cane 1987; Jin 1997). Earlier studies (Suarez and Schopf 1988; Battisti 1988) proposed a theory for ENSO cycle based on equatorial ocean wave dynamics and simplified coupling of winds and sea surface temperature, and they suggested that the equatorial wave dynamics is one of the key mechanisms for the ENSO development and decay. Jin (1997) simplified the theory by recognizing that at the low frequencies of ENSO, the ocean wave dynamics can be seen as leading to a recharge and discharge of equatorial heat content without needing explicit reference to the wave dynamics. Jin and An (1999) further demonstrated that it is

B. Huang (✉) · Y. Xue · H. Wang · W. Wang · A. Kumar
National Climate Data Center, Climate Prediction Center, NOAA, Asheville, NC 28801, USA
e-mail: boyin.huang@noaa.gov

Published online: 10 June 2011

largely the thermocline (mean vertical current) and zonal advective (anomalous zonal current) feedbacks that control the development and decay of ENSO.

Various studies have analyzed ENSO mechanisms based on direct observations (Hayes et al. 1991; Kessler and McPhaden 1995; Frankignoul et al. 1996; Picaut et al. 1996; Wang and McPhaden 2000, 2001; Vialard et al. 2001; Zhang and McPhaden 2006, 2008). While such observational analyses were often used to verify results from model simulations and theoretical studies, they are subject to uncertainties due to the sparseness of available data and imbalance in heat budget terms that are key physical processes. Particularly, there are no direct observations of vertical velocity due to its small magnitude, but it plays a critical role in ENSO development and decay. Ocean data assimilation combines observations and the first guess from the models, and has been found useful in characterizing ENSO-related processes (Kim et al. 2007; Huang et al. 2010). However, imbalances were introduced as part of the ocean data assimilation result in uncertainties in the ENSO diagnostics (Huang et al. 2010).

Another approach to understanding ENSO mechanisms is based on numerical simulations. Previous studies have used numerical models of various levels of complexity, including the Zebiak-Cane (ZC) type model (Schopf and Suarez 1988; Battisti and Hirst 1989; An and Jin 2001), ocean general circulation model (OGCM), and coupled GCM (Barnett and Latif 1991; Yu and Mechoso 2001; Yu and Liu 2003; Menkes et al. 2006; Zhang et al. 2007; An 2008; Zhang and McPhaden 2010). Given the importance of air-sea coupling and nonlinear interaction among different components in the ENSO dynamics, dynamically consistent datasets from coupled GCM simulations are especially useful for understanding the temporal and spatial variability and key mechanisms for ENSO. The disadvantage of the analysis of coupled GCM outputs for the ENSO studies is that conclusions can be subject to model biases. Nonetheless, analysis of such data still provides useful insights into various mechanisms that are responsible for ENSO variability, and helps advance our understanding.

The daily output from the Climate Forecast System (CFS; Saha et al. 2006) of the National Centers for Environmental Prediction (NCEP) is analyzed to understand ENSO variability and dominant mechanisms in this particular model. The CFS is a coupled ocean–atmosphere model that reproduces observed ENSO variability in the tropical Pacific with relatively realistic periodicity and spatial coherence (Wang et al. 2005). The NCEP CFS is used operationally predicting ENSO since 2004. This study, therefore, also helps enhance our understanding of the ENSO biases and prediction skill of this particular forecast system.

We diagnosed the ENSO mechanisms using mixed layer heat budget analysis, which follows the methodology of Huang et al. (2010). All thermodynamic and dynamic processes related to the ENSO evolution are analyzed. The analysis is stratified for different ENSO phases, allowing a quantification of the phase dependence of the contributing components. Given that various ENSO heat budget studies are monthly-mean fields (Kang et al. 2001; Zhang et al. 2007), it is unclear to what extent the results depend on the sampling of the output data. Availability of daily data also allows us to repeat the budget analysis with monthly means and helps us document degradation in resulting ENSO budget and related inferences.

The NCEP CFS is briefly described in Section 2. The methodology applied to the mixed layer heat budget is explained in Sect. 3. Results are presented in Sect. 4 for analysis based on daily-mean fields, and in Sect. 5 for analysis based on monthly–mean fields. A summary and discussion are provided in Section 6.

2 The NCEP CFS

The NCEP CFS has been described in detail by Saha et al. (2006). The atmospheric component of the CFS is the NCEP atmospheric Global Forecast System (GFS) model, with a spectral triangular truncation of 62 waves (about 200 km in the horizontal resolution) and 64 layers in vertical. The oceanic component of the CFS is the Geophysical Fluid Dynamics Laboratory (GFDL) Modular Ocean Model version 3 (MOM3) (Pacanowski and Griffies 1999). The ocean domain is quasi-global from 74°S to 64°N. The zonal resolution is 1°. The meridional resolution is 1/3° between 10°S and 10°N, 1° beyond 30°S and 30°N, and 1/3°–1° in between. There are 40 layers in the vertical with a bottom depth of 4.5 km. The vertical resolution is 10 m from the surface to the 240 m depth. The vertical mixing uses the nonlocal K-profile parameterization of Large et al. (1994). The atmospheric and oceanic components are coupled daily without flux adjustment. Poleward of 74°S and 64°N, the atmosphere is forced by observed SST climatology and there is no sea-ice model. The ocean initial conditions of 1 January 1981 were obtained from the Global Ocean Data Assimilation System (GODAS; Behringer and Xue 2004), which uses the same OGCM of CFS and has been operational at NCEP since 2003. The model was integrated for 60 years, and its daily outputs are used to analyze the mixed layer heat budget with a focus on the El Niño in the tropical Pacific at inter-annual timescale.

The CFS can well simulate the major ocean-atmospheric variabilities such as seasonal and interannual variations in the tropical Pacific (Pegion and Kirtman 2008; Jin et al. 2008). Major biases are that the warming in the boreal spring is delayed approximately 1-month in the tropical Pacific; the climatological SST is 1–3°C higher than

observations along the coast of Peru and southeastern tropical Pacific.

3 Methodology

3.1 Mixed layer depth

The criterion to calculate mixed layer depth (MLD) often differs based on requirements of the analysis (You 1995; Sprintall and Tomczak 1992; Huang et al. 2010). In this study, we define the MLD as the depth where the density is higher than that at the surface by 0.125 kg m^{-3}. We found that the mixed layer heat budget analysis is not sensitive to small changes of the density difference used to define the MLD.

The seasonal cycle of the MLD along the equator (1°S–1°N) is shown in Fig. 1a. The MLD is relatively shallow (deep) in the eastern (western-central) tropical Pacific. Seasonally, the MLD is relatively shallow (deep) in the boreal spring and fall (winter and summer) seasons in central eastern tropical Pacific. Compared with the MLD derived from ocean reanalyses such as GODAS and observations from World Ocean Atlas (WOA; Huang et al. 2010), the MLD in CFS is too shallow in the central tropical Pacific in the boreal summer and fall season (Jul–Nov). Also the CFS has a second minimum MLD in the boreal fall season, which is absent in GODAS and WOA.

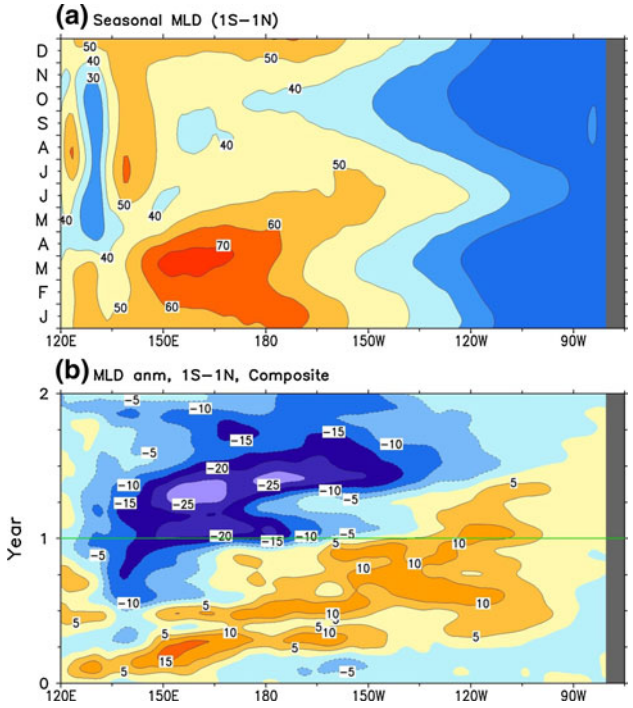

Fig. 1 **a** Climatological MLD along the equator (1°S–1°N). **b** Anomalous MLD along the equator for the composite El Niño. C.I. is 10 and 5 m in (**a**) and (**b**), respectively. 30-day running mean is applied

3.2 Temperature budget equation

The mixed layer temperature equation (Huang et al. 2010 and references therein) is expressed as:

$$T_t = Q_u + Q_v + Q_w + Q_q + Q_{zz}, \quad (1)$$

where T_t is the mixed layer temperature tendency, which is a sum of zonal advection (Q_u), meridional advection (Q_v), vertical entrainment (Q_w), net surface heat flux (Q_q), and vertical diffusion (Q_{zz}). Details of how to calculate these terms can be found in Huang et al. (2010). The weak horizontal diffusion was ignored in our analysis. To understand the physical processes controlling the temperature variations of the mixed layer on different time scales, each variable on the right hand side of Eq. 1 is decomposed into low frequency variation (>=75 day) and high frequency transient (hereafter referred to as eddy) following Kessler et al. (1998). With this decomposition, Eq. 1 becomes

$$T_t = Q_u^L + Q_v^L + Q_w^L + Q_q^L + Q_{zz}^L + E, \quad (2)$$

where superscript L represents the terms calculated with low-pass filtered variables and E represents the sum of high frequency eddies in longitudinal, latitudinal and depth directions (Huang et al. 2010). Eq. 2 is further decomposed into seasonal climatology (bar, see later Figs. 7, 13), which is the daily means averaged over the 60 years in the simulation, and anomaly from the seasonal mean (prime). The equation for anomalous temperature is, by omitting superscript L,

$$T_t' = Q_u' + Q_v' + Q_q' + Q_w' + Q_{zz}' + E', \quad (3)$$

and is used in the study of the anomalous temperature budget for a composite El Niño in our analysis.

A cutoff period of 75 days (Kessler et al. 1998) is chosen to separate seasonal and longer time scale variability from the eddy variability that is mainly associated with tropical instability waves (TIW; Contreras 2002; Jochum and Murtugudde 2006 and references therein). However, our analysis will show that some contribution from the Kelvin wave activity (30–90 day period; Kessler et al. 1995) is retained in the anomalous advective heat budget influencing the onset and termination of El Niño as indicated by Seo and Xue (2005).

3.3 Closure of temperature equation

To assess the physical mechanisms for an El Niño event using mixed layer temperature budget, it is useful to address if a reasonable closure of temperature budget is maintained using outputs from CFS. To demonstrate the closure of

mixed layer temperature budget, the correlation coefficient between T_t and forcing ($Q_u + Q_v + Q_w + Q_q + Q_{zz}$) is calculated using daily temperature budget of 60 years. Figure 2 shows that the correlation coefficient is above 0.9 in most of the tropical Pacific for both total (Eq. 2) and anomalous (Eq. 3) budgets. The correlation is relatively low (near 0.8) in the eastern equatorial Pacific, and it may be associated with the defects of parameterizations of vertical entrainment and diffusion. In the NINO3.4 region (5°S–5°N, 170°W–120°W), the correlation between area averaged temperature budgets is higher than 0.97 for both seasonal climatology and the anomaly (Fig. 3). Similarly, a high correlation of 0.95 (not shown) is found in NINO3 (5°S–5°N, 150°W–90°W) and NINON4 (5°S–5°N, 160°E–150°W) regions. This indicates that the temperature budgets described by Eqs. 1–3 have a good closure, ensuring that the results regarding the mechanisms controlling the El Niño development are robust.

4 Composite temperature budget of El Niño

4.1 El Niño composite

Figure 4a shows monthly anomaly of the mixed layer temperature at NINO3.4 region in CFS. Monthly mean

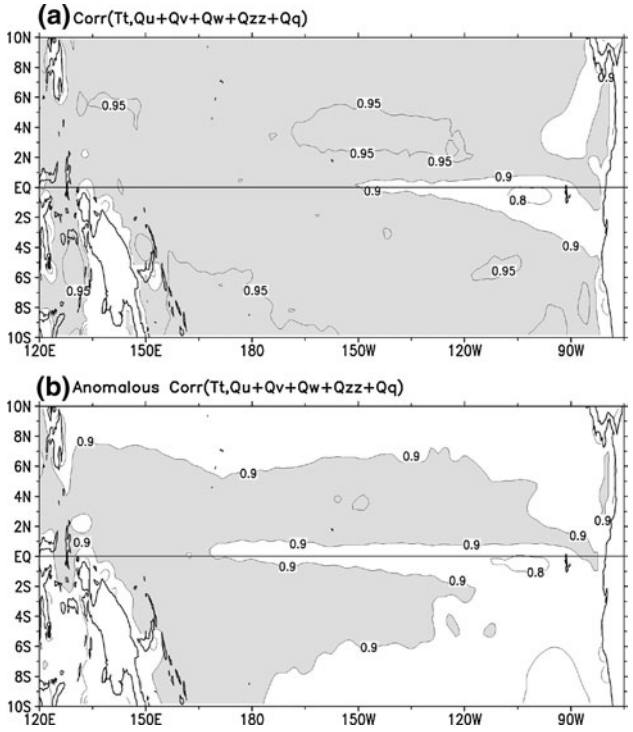

Fig. 2 Correlation coefficients between **a** T_t and $Q_u + Q_v + Q_w + Q_{zz} + Q_q$, and **b** Anomalous T_t and $Q_u + Q_v + Q_w + Q_{zz} + Q_q$. Contours are 0.8, 0.9, and 0.95. Contour values of 0.9 or higher are *shaded*

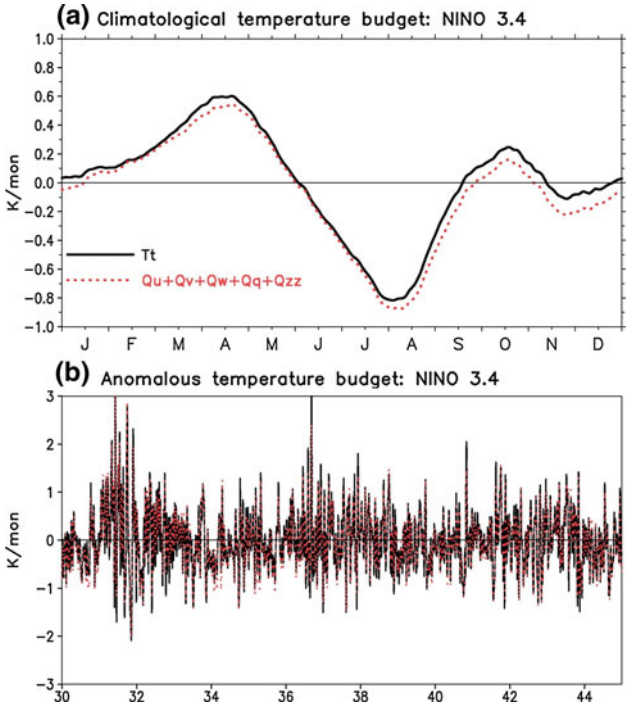

Fig. 3 **a** Climatological (year 1–60) temperature budget closure at NINO3.4 region (5°S–5°N, 170°–120°W). **b** Anomalous temperature budget closure that is only partially displayed from year 30 to 45. A 7-day running mean is applied in (**b**). The correlation coefficient between T_t and the forcing ($Q_u + Q_v + Q_w + Q_{zz} + Q_q$) is 0.995 and 0.97 in (**a**) and (**b**), respectively

anomaly is used to define an El Niño event using traditional NINO3.4 SST anomaly (SSTA) index (which is close to the mixed layer temperature anomaly). Figure 4 demonstrates the capability of CFS in simulating the ENSO frequency (Fig. 4a), magnitude (Fig. 4b), and spatial distribution (Fig. 4c) in the tropical Pacific. In the subsequent analysis, a criterion of 1.5°C anomaly is selected to define El Niño events. During the 60-year simulation, eight El Niño events (Fig. 4b; Table 1) are identified. It is found that the maximum anomaly of composite mixed layer temperature is located near 120°W during the development (Fig. 5i) and the mature phase (Jan of year 1; Fig. 4c). In contrast, observed maximum SSTA is located near the western coast of South America during the development phase, propagates westward, and reaches at 120°W in the mature phase (Rasmusson and Carpenter 1982). The peak amplitude for the El Niños, in general, is phase-locked to the boreal winter as in the observations (Rasmusson and Carpenter 1982; Tziperman et al. 1998; Galanti and Tziperman 2000). The peak phase occurred as early as September, as occasionally seen in observations (for example, the 1986–88 El Niño; McPhaden et al. 1990). To construct an El Niño composite, all the El Niño events are aligned according to their peak phases which are reset to be Jan of year 1 after the alignment (Fig. 4b), similar to the treatment

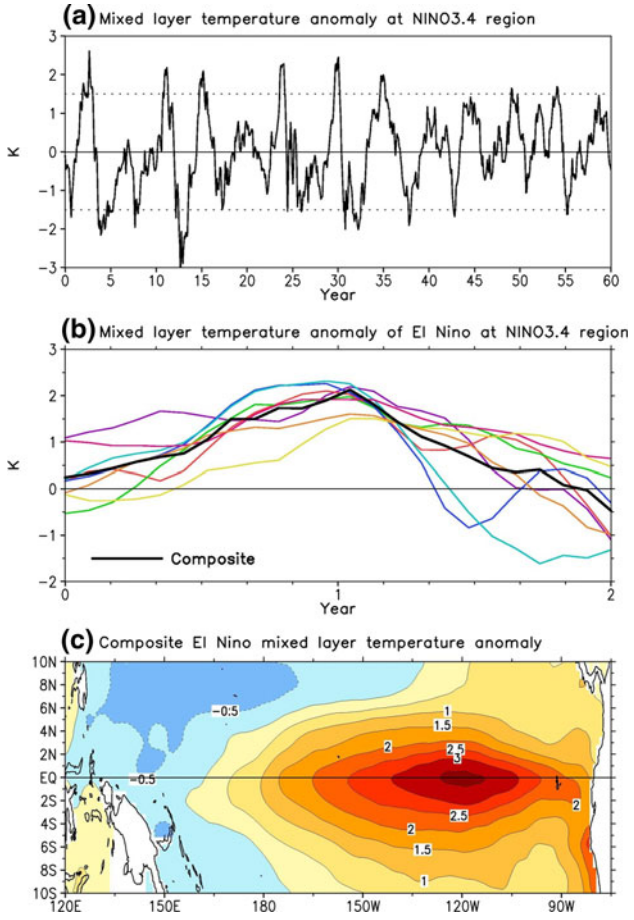

Fig. 4 **a** Monthly mixed layer temperature at NINO3.4 region. The *horizontal dashed line* at 1.5°C is used as a criterion to select El Niño events. The El Niño events and their maximum temperature anomalies are listed in Table 1. **b** Temperature evolutions of El Niño composite members at NINO3.4 region. **c** Mixed layer temperature anomaly of composite El Niño at Jan of year 1. Contour interval is 0.5°C

in Zhang et al. (2007). For convenience of discussion, we refer Jan–Mar of year 0, Apr–Dec of year 0, Jan–Jun of year 1, and Jul–Dec of year 1 to the time of El Niño onset, development, decay, and phase transition, respectively.

4.2 SST, wind stress, and surface ocean current

Various features of the El Niño composite are shown in Fig. 5, and their spatial structure helps frame the discussion for the El Niño budget. As positive SSTA appears in the east-central equatorial Pacific (Fig. 5i), anomalous westerly wind (Fig. 5a) begins to emerge in Jan of year 0, propagates eastward, and strengthens during entire El Niño development phase. Corresponding to the anomalous westerly wind, precipitation is enhanced in the central tropical Pacific near the dateline (Fig. 5d); anomalous surface zonal current (Fig. 5e), downwelling (Fig. 5g), and sea surface height (SSH; Fig. 5h) develop and propagate eastward throughout year 0. The changes in meridional wind (Fig. 5b) and current (Fig. 5f) are relatively weak near the equator. In the decay and transition phase of year 1 (Fig. 5i), the westerly wind anomaly gradually weakens in the central equatorial Pacific (Fig. 5a), although a tendency for eastward propagation continues. The continued eastward propagation is likely due to the seasonal cycle of SST in the eastern Pacific that reaches its maximum amplitude in boreal spring, and an eastward shift in the warmer total SST (i.e., the sum of SST climatology and the anomalous SST) also results in an eastward shift in precipitation (Fig. 5d). It is also noteworthy to point out that around the peak phase of El Niño, an easterly wind anomaly emerges in the western equatorial Pacific in Dec of year 0, and strengthens in Jan–Mar of year 1.

It is interesting to note that variations with periods of 90–120 days exhibits in eastward surface zonal current anomalies (Fig. 5e) despite of averaging of eight events. Those variations might be related to intraseasonal variability in CFS, which has periods about 60–80 days and amplitude about double of that in observations (Wang et al. 2005). Intraseasonal variability in CFS is particularly too strong in the central and eastern Pacific (Wang et al. 2005), which will be shown in the composite of the mixed layer zonal advection (later Fig. 7a) and temperature tendency (later Fig. 7e) in the NINO3.4 region.

The anomalous surface current changes directions abruptly from eastward to westward in Jan of year 1, and propagates eastward to the central and eastern equatorial Pacific subsequently (Fig. 5e). The sudden onset of anomalous westward zonal current can be attributed to the rapid weakening (strengthening) of westerly (easterly) wind anomaly in the central (western) equatorial Pacific (Fig. 5a), which tends to reduce the equatorial heat content by forcing upwelling oceanic Kelvin waves (Schopf and Suarez 1988). When the equatorial heat content decreases rapidly through oceanic Kelvin wave processes (Fig. 5h), a

Table 1 Eight selected El Niños from 60 year CFS simulation

Year	3	12	16	25	31	35	50	55
Month	Sep	Mar	Mar	Jan	Jan	Dec	Jan	Jan
Max SST (°C)	2.6	2.2	2.1	2.3	2.5	2.0	1.6	1.7

"Year" and "Month" represent the time for an El Niño event reaching its maximum sea surface temperature anomaly

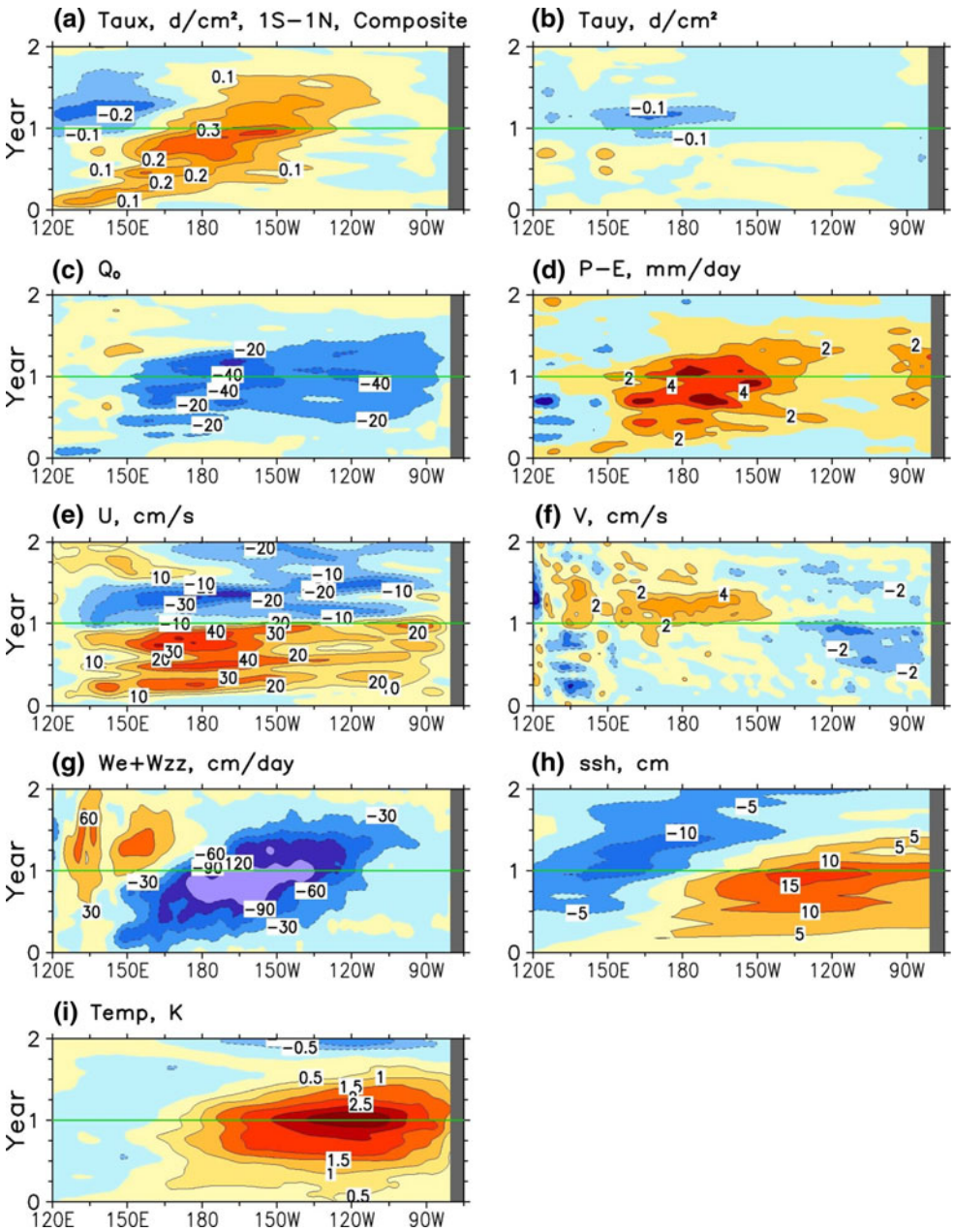

Fig. 5 Anomalies of the El Niño composite along the equator (1°S–1°N). **a** Zonal wind stress, **b** Meridional wind stress, **c** Net surface heat flux, **d** P-E, **e** Zonal and **f** Meridional current in the mixed layer, **g** Vertical entrainment velocity, **h** Sea surface height, and **i** Mixed layer temperature. C.I. is 0.1 dyne cm^{-2} in (**a**) and (**b**), 20 W m^{-2} in (**c**), 2 mm day^{-1} in (**d**), 10 cm s^{-1} in (**e**), 2 cm s^{-1} in (**f**), 30 cm day^{-1} in (**g**), 5 cm in (**h**), and 0.5°C in (**i**)

strong equator-ward gradient of SSH anomaly forms, which forces surface water to move westward through geostrophic adjustment.

Associated with a positive SST anomaly in the central eastern tropical Pacific, the heating from the net atmospheric heat flux reduces (Fig. 5c). Therefore, the heating to the mixed layer (Q_q[1]; Figs. 6f, 7a) tends to damp the El Niño development due to its negative correlation with mixed layer temperature anomaly, as suggested by Wang and McPhaden (2000, 2001).

[1] Q_q is defined as net surface heat flux (Fig. 5c) divided by mixed layer depth (Fig. 1b). See details in Huang et al. (2010).

4.3 Zonal advective feed back

Our analysis of daily temperature budget shows that zonal advection plays an important role in the onset and development of the composite El Niño in the CFS, consistent with the results in observational and modeling studies (Frankignoul et al. 1996; Picaut et al. 1996; Wang and McPhaden 2000, 2001; An and Jin 2001; Vialard et al. 2001; Zhang et al. 2007; Huang et al. 2010). Shown in Fig. 6 are the various forcing terms for the tendency of mixed layer temperature, which can be thought as the convolution of composite anomalies and various gradients—zonal, meridional, and vertical (Fig. 5).

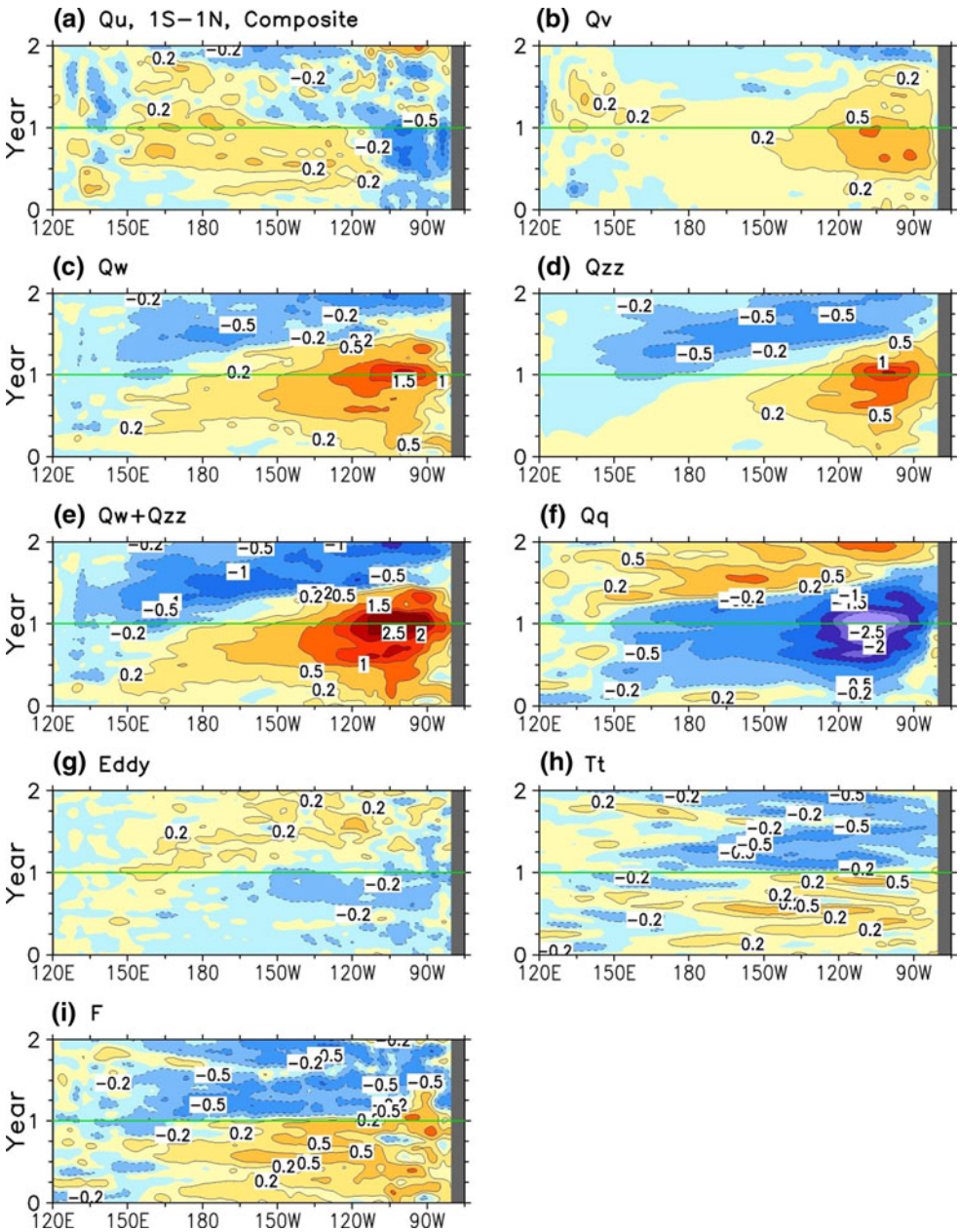

Fig. 6 Low-pass filtered temperature budgets of the El Niño composite between 1°S and 1°N by **a** Zonal advection, **b** Meridional advection, **c** Entrainment, **d** Vertical diffusion, **e** Entrainment and vertical diffusion, and **f** Net surface heat flux. **g** Eddy between unfiltered and low-pass filtered budgets. **h** Unfiltered temperature tendency, and **i** Unfiltered forcing. Contours are 0, ±0.2, ±0.5, ±1, ±1.5, ±2, and ±2.5°C mon^{-1}. A 30-day running mean has been applied in the plots

Figure 6a shows that anomalous warming by zonal advection emerges in the central equatorial Pacific near the dateline in February of year 0. The contribution from the zonal advection is directly associated with eastward zonal current (Fig. 5e) in the equatorial Pacific that results from a positive feedback between SSTA (Fig. 5i) and changes in convection and anomalous zonal wind stress (Bjerknes 1969; Jin 1997; Jin and An 1999).

A switch in the direction of anomalous zonal current after Jan of year 1 (Fig. 5e) clearly demarks the beginning of the El Niño decaying phase. This can be seen in the area averaged temperature budget in the NINO3.4 region (Fig. 7a) where Nino3.4 SST anomalies peak around this time, and start to decline thereafter.

To gain further insight, we analyze the decomposition of temperature tendency due to zonal advection into its components. The decomposition of zonal advective temperature tendency (Fig. 7b) indicates that the contribution of zonal advection to the development and decay of the El Niño is largely associated with anomalous zonal current ($-u' \cdot \bar{T}_x$), which is consistent with the concept of the zonal advective feedback (Jin and An 1999).

The mean zonal current ($-\bar{u} \cdot T'_x$) also contributes to the El Niño development, although its role is weaker than the

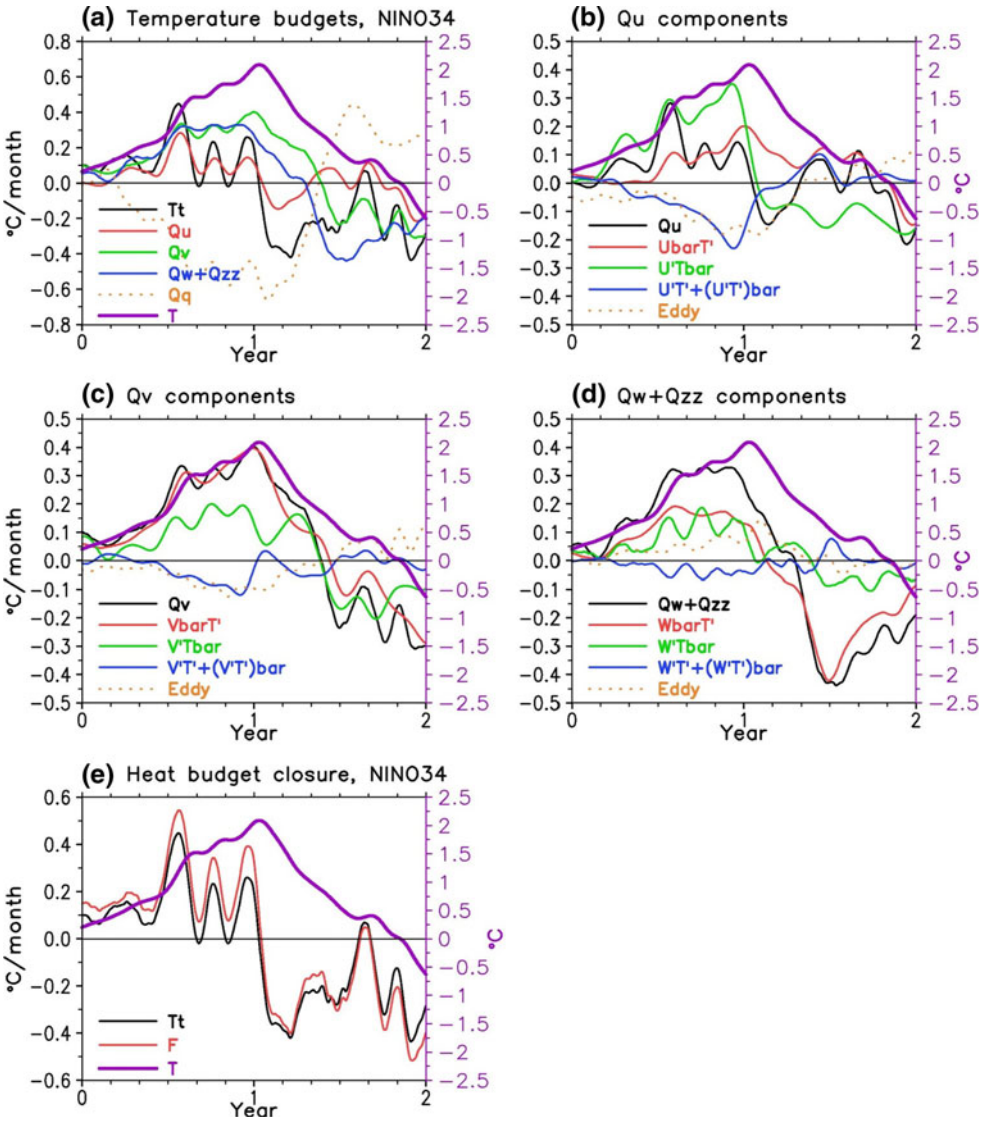

Fig. 7 Temperature budget anomalies of the El Niño composite in NINO3.4 region (5°S–5°N, 120°W–170°W). **a** Unfiltered temperature budgets (°C mon^{-1}). Decomposition of low-pass filtered **b** Zonal advection, **c** Meridional advection, **d** Entrainment and vertical diffusion, and **e** Temperature budget closure. The unfiltered budgets in (**a**) are replotted in (**b**–**e**). Temperature anomalies are plotted in the scale of the right axis. Decomposed climatology and associated anomaly are noted as bar and prime, for example, $\bar{U}T' = -\bar{u} \cdot T'_x$. The terms such as $U'T' = -u' \cdot T'_x$ represent the non-linearity. The "Eddy" in (**b**–**d**) represents the difference between unfiltered budget anomaly in (**a**) and low-pass filtered budget anomaly. A 30-day running average is applied in plots

anomalous current. The non-linear ($-u' \cdot T'_x$) and eddy terms tend to damp the El Niño development. The damping effect from the eddy can be largely attributed to the TIW activities, and is in concordance with previous studies (Yu and Liu 2003; Zhang and McPhaden 2010). On the other hand, the damping effect from the non-linear term appears to be in contradiction to Jin et al. (2003) and An and Jin (2004) who showed a direct contribution of non-linear heating to the development of the extremely strong El Niño in 1997–98. The difference may be due to the fact that our composite El Niño cannot represent an extremely strong El Niño event. Another possible reason for the difference is their use of monthly averaged data, and will be discussed in Sect. 5.

Further details about the contribution of zonal advective tendency are illustrated for the El Niño development phase of the month of July (year 0) (Fig. 8). The contribution of mean and anomalous zonal current displayed in Fig. 8a and b clearly show that both terms contribute to the warming of the mixed layer in the tropical Pacific west of 110°W, although the role of mean zonal current is relatively weak between 180° and 110°W. Further, both components of the zonal advection contribute to a cooling east of 110°W.

The spatial structure of zonal advective heating and cooling result from combined effects of zonal gradients of mean (Fig. 9a) and anomalous (Fig. 9d) mixed layer temperature, as well as signs of mean (Fig. 9g) and anomalous (Fig. 9j) zonal current of the mixed layer. The signs of zonal gradient of mean and anomalous temperature are approximately opposite west and east of 110°W, while signs of mean (Fig. 9g) and anomalous (Fig. 9j) surface current are uniform in the tropical Pacific. This is why the

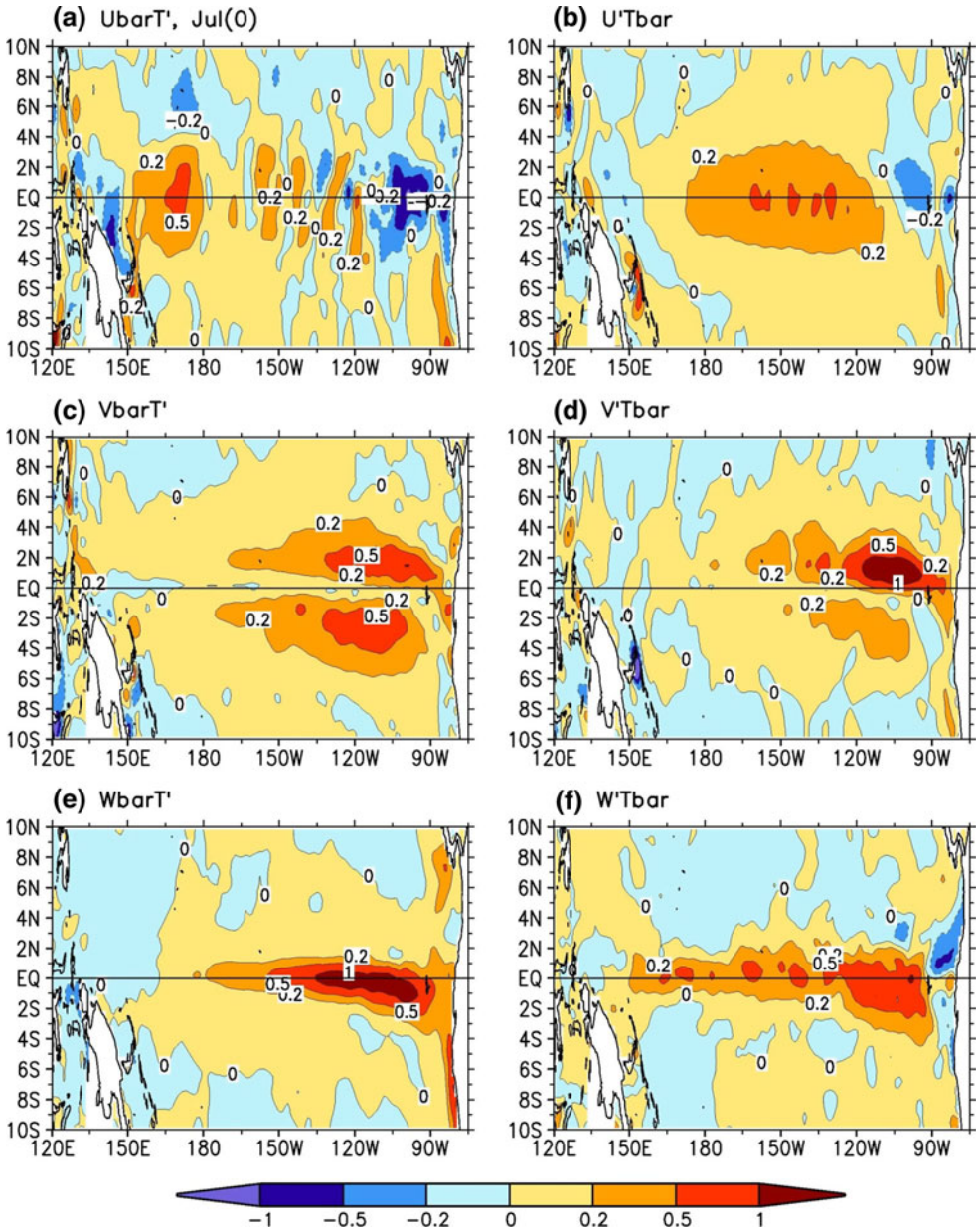

Fig. 8 Temperature budget distributions in Jul of year 0. **a** $-\bar{u}T'_x$, **b** $-u'\bar{T}_x$, **c** $-\bar{v}T'_y$, **d** $-v'\bar{T}_y$, **e** $-\bar{w}T'_z$, and **f** $-w'\bar{T}_z$. Contours are 0, ±0.2, ±0.5, and ±1°C mon^{-1}

combined zonal advection by both mean and anomalous zonal current contributes to a warming (cooling) west (east) of 110°W. As a result, the contributions from zonal advection (Fig. 8a, b) become weaker in the NINO3 region (150°W–90°W) because of cancellation of heating (150°W–110°W) and cooling (110°W–90°W).

The damping effect from non-linear term can also be seen in the central-western Pacific west of 110°W due to eastward anomalous current (Fig. 9j) and positive zonal gradient of anomalous temperature (Fig. 9d), and therefore their combined effect is a cooling. The non-linear term indeed contributes to the El Niño development in the far east equatorial Pacific east of 110°W due to eastward anomalous current (Fig. 9j) and negative gradient of anomalous temperature (Fig. 9d), which is consistent with Jin et al. (2003) and An and Jin (2004).

4.4 Vertical advective feedback

Many studies (Hayes et al. 1991; Kessler and McPhaden 1995; Jin 1997; Jin and An 1999; Wang and McPhaden 2000, 2001; Zhang and McPhaden 2006, 2008; Kim et al. 2007; Zhang et al. 2007) showed that vertical advection of temperature contributes to the El Niño onset, development, decay, and phase transition. Consistent with these studies, our analysis of CFS simulation also shows that vertical

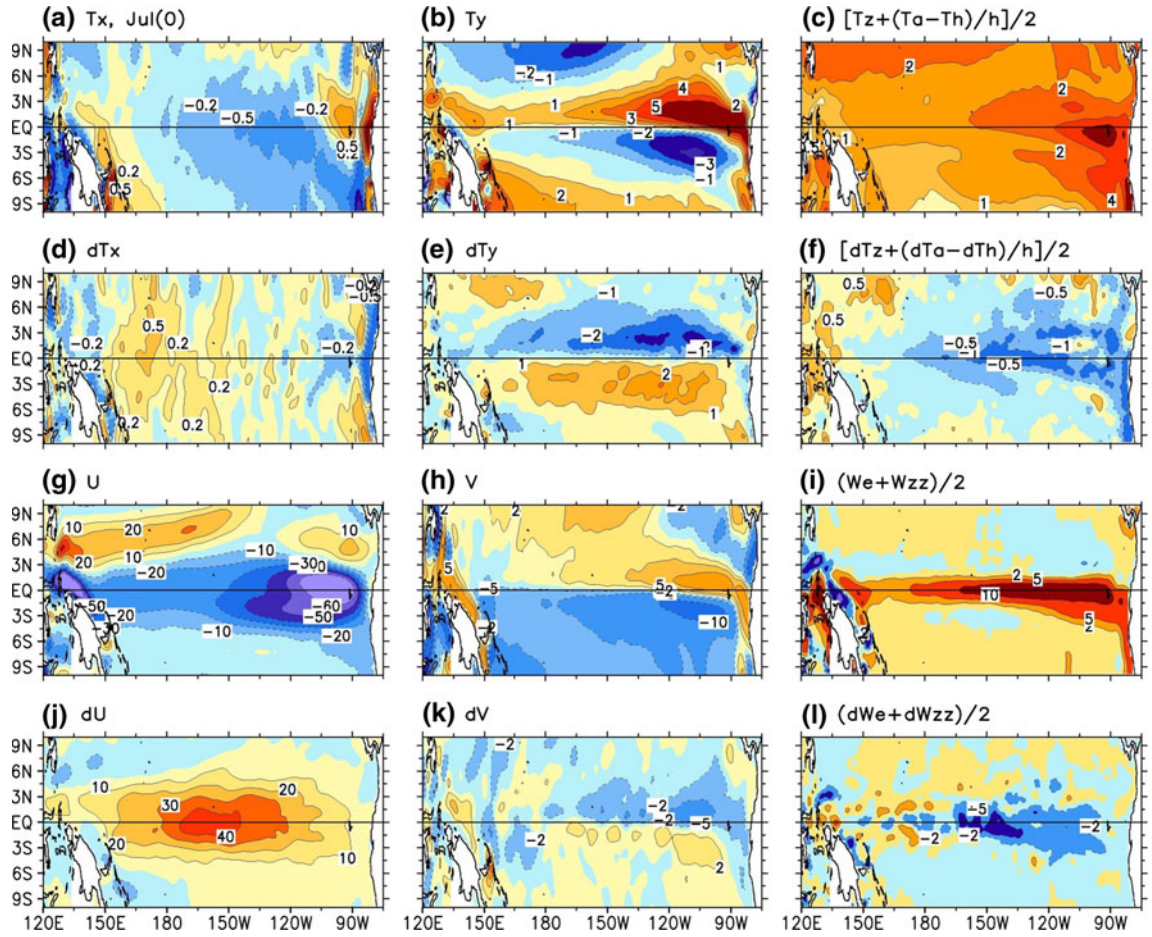

Fig. 9 Climatological temperature gradient in **a** zonal, $\bar{T}_x$, **b** meridional, $\bar{T}_y$, and **c** vertical, $\bar{T}_z$, in the mixed layer in Jul of year 0. Anomalous temperature gradient in **d** zonal, T'_x, **e** meridional, T'_y, and **f** vertical, T'_z, in Jul of year 0. Climatological current in **g** zonal, $\bar{u}$, **h** meridional, $\bar{v}$, and **i** vertical, $\bar{w}$, in Jul of year 0. Anomalous current in **j** zonal, u', **k** meridional, v', and **l** vertical, w', in Jul of year 0. Contours are 0, ±0.2, ±0.5, and ±1 × 10^{-6} °Cm^{-1} in (**a**) and (**d**). C.I. is 1 × 10^{-6} °Cm^{-1} in (**b**) and (**e**). Contours are 0, ±0.5, ±1, ±2, ±4, and ±6×10^{-2} °Cm^{-1} in (**c**) and (**f**). C.I. is 10 cms^{-1} in (**g**) and (**j**). Contours are 0, ±2, ±5, and ±10 cms^{-1} in (**h**) and (**k**); and 0, ±2, ±5, and ±10 × 10^{-6} m s^{-1} in (**i**) and (**l**)

advection of temperature plays a critical role in the onset, development, decay, and phase transition of the El Niño.

Figure 5g shows that anomalous downwelling[2] at the bottom of mixed layer emerges at the onset stage of the El Niño, which is directly associated with anomalous Ekman convergence from the anomalous eastward currents. This anomalous downwelling directly contributes to the warming in the western equatorial Pacific (Fig. 6c, d, e), and propagates eastward along with other components of the coupled ocean–atmosphere system such as mixed layer temperature anomaly (Fig. 5i), anomalous zonal wind stress (Fig. 5a), zonal surface current (Fig. 5e), and SSH (Fig. 5h). Therefore, the anomalous downwelling is one of the important components for the El Niño development (Bjerknes 1969). The overall contribution from vertical advection (Fig. 6e) exceeds that from zonal advection (Fig. 6a) during the onset and development phase of the El Niño, and is better depicted in the NINO3.4 region (Fig. 7a). This result is similar to the GODAS reanalysis (Huang et al. 2010).

In the decay and transition phases, a cooling from vertical advection and diffusion ($Q_w + Q_{zz}$) (Fig. 6e) appears in the western equatorial Pacific, which is consistent with the sign switch of anomalous zonal wind stress (Fig. 5a) and associated Ekman divergent flow and anomalous upwelling (Fig. 5g) in the western equatorial Pacific in Jun of year 1. In the central-eastern equatorial Pacific, the heating by vertical advection and diffusion weakens dramatically after Jan of year 1 (Fig. 6e), and contributes further to the decay of the El Niño. This can be seen clearly in NINO3.4 region (Fig. 7a). The rapid

[2] The vertical current at the bottom of the mixed layer is defined (Wang and McPhaden 2000) as the combination of entrainment velocity W_e and equivalent diffusive velocity $W_{zz} = K_z/h$; where K_z is vertical diffusivity and h is mixed layer depth. See details in Huang et al. (2010).

weakening of heating by vertical advection and diffusion contributes to a large portion of the cooling of the mixed layer between Jan and Jun of year 1. The role of anomalous vertical advection and diffusion changes from a heating to a cooling in Jul of year 1, 5 months after zonal advection switches its sign. This is different from the GODAS reanalysis (Huang et al. 2010) where the cooling by zonal advection dominates.

Analysis of the various components of the vertical advective tendency shows that both mean and anomalous vertical current contribute to the El Niño development. The decomposition of vertical temperature budget in NINO3.4 region (Fig. 7d) shows that mean $(-\bar{w} \cdot T_z')$ and anomalous $(-w' \cdot \bar{T}_z)$ vertical current contribute about equally to the El Niño development before Jan of year 1. Therefore, they form a combined vertical advective feedback. The former process associated with mean upwelling is called thermocline feedback by Jin (1997) and Jin and An (1999). In the decay and transition phase, however, the mean vertical current contributes dominantly to the cooling after Jun of year 1. This appears to be consistent with the theory of thermocline feedback (Jin and An 1999), but different from the dominant role of anomalous zonal current in GODAS reanalysis (Huang et al. 2010). In addition, the non-linear term weakly damps the warming during the El Niño development, which is different from the analysis of Jin et al. (2003). The vertical eddy component also tends to weakly enhance the warming during the El Niño development in contrast to a negative tendency due to zonal eddies (and also in the meridional direction as would be discussed in the following subsection), which is consistent with the simulation of Menkes et al. (2006).

A more detailed look at the spatial structure of tendency due to vertical velocity is made for July (year 0). The contribution from mean and anomalous vertical current is almost equally strong and confined within a narrow band of the equatorial Pacific during the El Niño development (Fig. 8e, f). The reason for the warming within a narrow equatorial band is that both mean and anomalous vertical current is confined within a narrow band of the equatorial Pacific (Fig. 9i, l). The reasons for equally important contributions from mean and anomalous vertical current in the equatorial Pacific are (1) vertical gradient[3] of mean temperature is strong (Fig. 9c) but anomalous vertical current is weaker (Fig. 9l), and (2) vertical gradient of anomalous temperature is weak (Fig. 9f) but mean vertical current is strong (Fig. 9i). However, mean upwelling indeed contributes dominantly to the vertical advection of temperature in the NINO3 region (not shown) because of stronger and broader mean vertical upwelling (Fig. 9i). This is in agreement with thermocline feedback theory (Jin and An 1999). In addition, the reason for non-linear term in damping the El Niño development is clear, since the combined vertical advection from negative vertical gradient of anomalous temperature (Fig. 9f) and anomalous downwelling (Fig. 9l) results in a cooling.

4.5 Meridional advective feedback

Besides zonal and vertical advective feedbacks, the meridional advection of temperature also plays an important role in the onset, development, decay, and phase transition of the El Niño in CFS as indicated in the studies of model simulations and ocean reanalyses (Battisti 1988; Barnett and Latif 1991; Yu and Mechoso 2001; Zhang et al. 2007; Huang et al. 2010). Figure 6b shows that meridional advection of temperature contributes to the warming in the central-eastern equatorial (1°S–1°N) Pacific east of 150°W during the El Niño development between Mar and Dec of year 0. However, the meridional advection is very weak in the central-western equatorial Pacific west of 150°W during this period. The reasons for a weak meridional advection in El Niño development (e.g. Jul of year 0) in the central-western equatorial Pacific are (1) anomalous meridional current (Fig. 5f) is weak in the central-western equatorial Pacific, which is more evident in the El Niño development period in Fig. 9k; (2) mean meridional current (Fig. 9h) is weak; and (3) meridional gradients of both mean (Fig. 9b) and anomalous (Fig. 9e) temperature are weak along the equator.

The role of meridional advection, however, is evident in the off-equatorial tropical Pacific. In fact, Fig. 7a shows that the contribution from the meridional advection in NINO3.4 region is larger than that from zonal advection, and is comparable to that from vertical advection during the El Niño development. In the decay phase, meridional advection also contributes to the cooling of the mixed layer. The warming by meridional advection decreases as fast as that by vertical advection and diffusion from Jan to Jun of year 1, although it is not as fast as that by zonal advection between Dec of year 0 and Feb of year 1. Furthermore, the decomposition of the meridional advection (Fig. 7c) shows that both mean $(-\bar{v} \cdot T_y')$ and anomalous $(-v' \cdot \bar{T}_y)$ meridional current contribute to the El Niño development, decay, and phase transition. In addition, nonlinearity and eddy tend to damp the El Niño development, which is quite similar to those in zonal direction shown in Fig. 7b.

[3] The vertical gradient of temperature is define as the average of the gradient at the bottom of the mixed layer $[T_z(z = h)]$ and the equivalent gradient $[T_a - T_h/h]$, where T_a and T_h are the temperature within and at the bottom of the mixed layer, respectively. See details in Huang et al. (2010).

Further analysis confirms that the contribution of meridional advection to the El Niño development (e.g. Jul of year 0) in NINO3.4 region results from both mean (Fig. 8c) and anomalous (Fig. 8d) meridional current in the off-equatorial central-eastern tropical Pacific. The advection by mean and anomalous meridional current is approximately symmetric about the equator, and is strongest in the eastern tropical Pacific near 1°N and 2°S. In the south-eastern tropical Pacific, the advection associated with anomalous meridional current is relatively weak (Fig. 8d). Both mean and anomalous advections are directly associated with strong meridional gradients of mean (Fig. 9b) and anomalous (Fig. 9e) temperature. These meridional gradients are almost 10 times larger than the zonal gradients of mean (Fig. 9a) and anomalous (Fig. 9d) temperature in the off-equatorial tropical Pacific. However, the magnitude of mean (Fig. 9h) and anomalous (Fig. 9k) meridional current is almost 10 times smaller than that of mean (Fig. 9g) and anomalous (Fig. 9j) zonal current in the off-equatorial tropical Pacific. Therefore, the meridional temperature advection by mean and anomalous meridional current is of the same magnitude as the zonal temperature advection. In addition, from the anti-symmetric north–south distributions of anomalous meridional temperature gradient and anomalous meridional current, it is easy to see why their combined effect of non-linearity is a cooling and tends to damp the El Niño development. This leads to a conclusion that is different from the analysis of Jin et al. (2003).

Since meridional advection plays a critical role in the onset, development, decay, and phase transition of the El Niño in the coupled CFS model simulation, we propose a meridional advective feedback that works similar to the zonal and vertical advective feedbacks. For an initial SST anomaly in the western tropical Pacific, the response of the atmosphere is a westerly wind anomaly to the west of the SST anomaly (Gill 1980). The westerly wind anomaly generates an anomalous eastward current and downwelling that form zonal and vertical advective feedbacks. At the same time, westerly wind anomaly also induces an anomalous equatorward convergent flow (Fig. 9k) that enables a heating to enhance the initial SST anomaly due to positive and negative meridional gradient of mean temperature straddling the equator (Fig. 9b). Similarly, the poleward divergent mean current (Fig. 9h) also enables a heating to strengthen the initial SSTA due to negative and positive meridional gradients of anomalous temperature straddling the equator (Fig. 9e). These descriptions indicate that both the mean and anomalous meridional currents tend to enhance the initial positive SST anomaly. Therefore we can combine these two effects into a single meridional feedback such as zonal and vertical advective feedbacks.

4.6 Phase transition of El Niño

The positive feedbacks in zonal, vertical, and meridional directions described above suggest that the onset and development of the El Niño involve complicated changes of 3-dimensional ocean–atmosphere system. In the presence of positive feedbacks a question is how does the El Niño transit from mature phase to a La Niña?

Figure 10 shows the vertical cross section of the evolution of temperature and ocean circulation at the equator following the El Niño evolution. During the early development stage, a westerly wind anomaly, e.g., in Apr-Jun of year 0 (Fig. 5a), results in near surface easterly currents and a downwelling in east of 150°E due to Ekman convergence. In response to the eastward and downward current near the surface, the thermocline water diverges and upwells in the western Pacific, which results in a negative thermocline temperature anomaly and shallowing 20°C isotherm depth. The cooling in the thermocline of the western tropical Pacific gradually penetrates eastward and upward to the eastern tropical Pacific (Fig. 10b, c, d, e), while 20°C isotherm flattens (shallower in the west and deeper in the east) and anomalous current strengthens. The cooling in the tropical thermocline eventually flips the vertical, zonal, and meridional advective feedbacks after the mature phase leading to El Niño decay after Jan of year 1.

The above descriptions of the changes in the equatorial oceanic circulation are consistent with the conceptual framework of the recharge discharge mechanism for ENSO variability discussed by Jin (1997) and Jin and An (1999). To verify their hypothesis, we calculate the mixed layer temperature anomaly, which is close to SSTA, in the eastern tropical Pacific NINO3 region (T_e) and the mean thermocline depth (20°C isotherm depth) anomaly across the entire tropical Pacific (5°S–5°N, 120°E–85°W; H_m). It is found that H_m leads T_e by 5–7 months and their correlation coefficient is approximately 0.9, which is consistent with observational studies of Wrytki (1975) and Meinen and McPhaden (2000).

5 Temperature budget using monthly outputs

The temperature budget analysis in the previous section provides a means to diagnose the physical mechanisms controlling the El Niño. It is demonstrated that the diagnosis using daily averaged outputs provides a good closure of temperature budget as shown in Figs. 2 and 3. However, as the temporal resolution of the output data becomes coarse, e.g. using monthly outputs (Jin et al. 2003; Zhang et al. 2007), the diagnosis may fail to resolve high frequency variability such as oceanic Kelvin waves and TIW

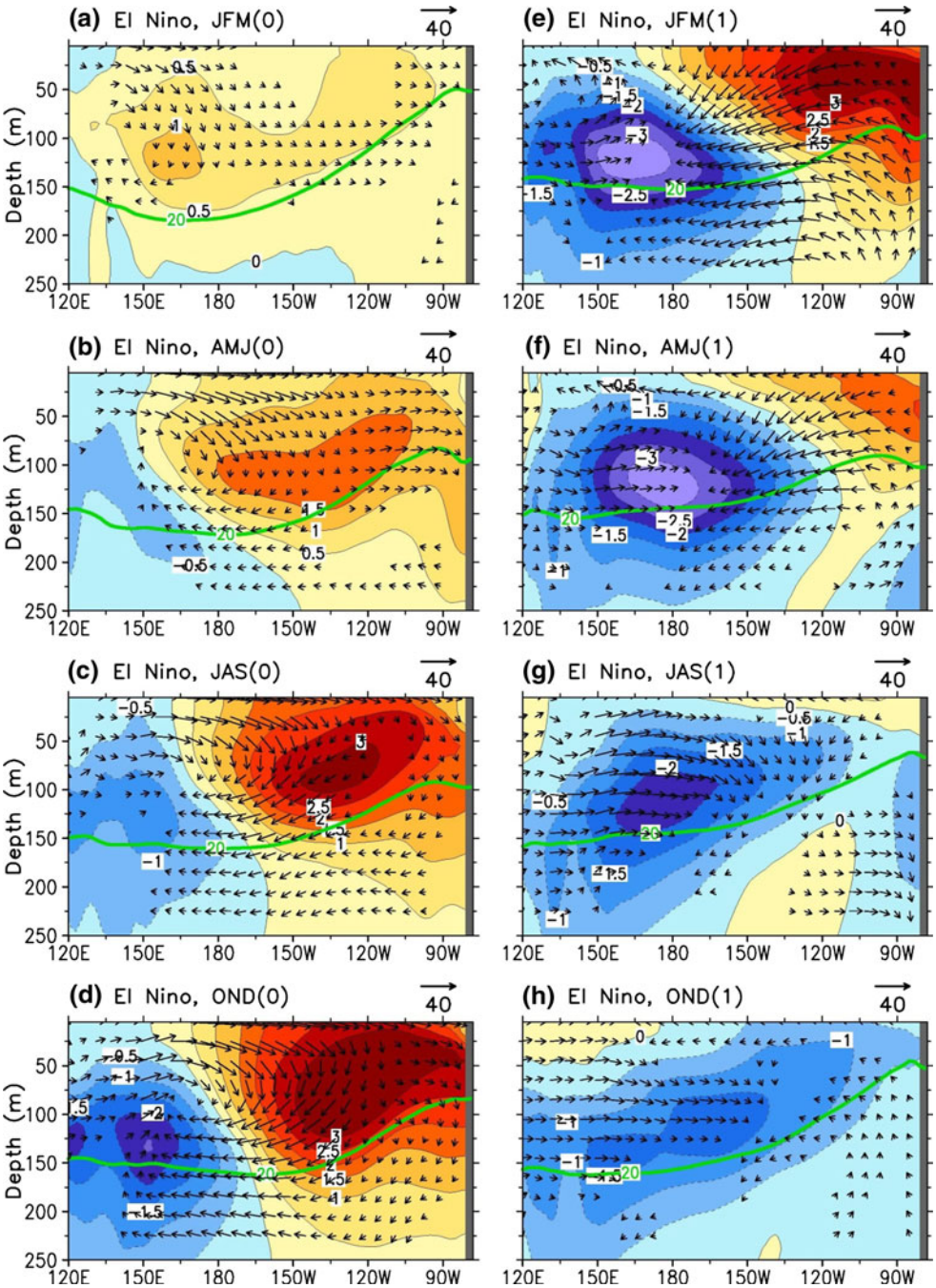

Fig. 10 Seasonal evolution of anomalous temperature (*shading*) and currents (*vectors*) in the equatorial (1°S–1°N) Pacific, and 20°C isotherm (*green contour*) in the tropical (5°S–5°N) Pacific. The vertical velocity is amplified according to the scale ratio of longitudinal basin size (155°) and depth (250 m). The number in the parenthesis of the subtitle is indicates the year of El Niño development

and to close the temperature budget. This may contaminate a meaningful diagnosis.

To assess the influence of different temporal averages on the ENSO budget diagnostics, we repeated the temperature budget analysis using monthly outputs that are averaged from original daily outputs. Figure 11 shows the correlation coefficient between T_t and forcing ($Q_u + Q_v + Q_w + Q_q + Q_{zz}$) for total and anomalous temperature budget. It is clear that the correlation coefficient reduces dramatically in the tropical Pacific, particularly in the eastern equatorial Pacific in comparison with that using daily outputs (Fig. 2). The correlation is higher than 0.8 when daily outputs are used in Fig. 2, but it reduces to 0.2–0.6 when monthly outputs are used (Fig. 11). The correlation increases when an area average is applied as in the case using daily outputs. In the NINO3.4 region, for example, the correlation coefficients increase to 0.92 and 0.74 for the temperature budget at seasonal and interannual timescales, respectively (Fig. 12). Nevertheless, these correlation coefficients are significantly lower than their counterparts (0.995 and 0.97, respectively) using daily outputs (Fig. 3).

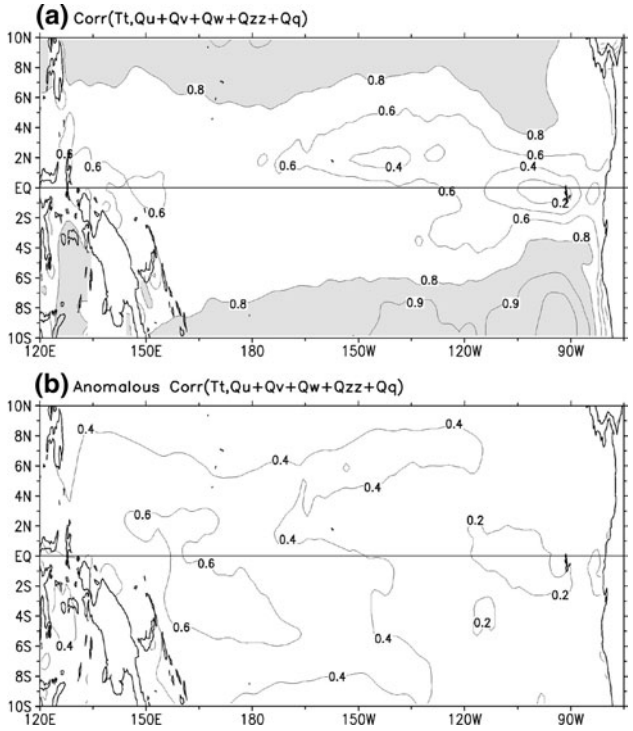

Fig. 11 Same as Fig. 2 except for temperature budget calculated using monthly averaged variables. Contours are 0.2, 0.4, 0.6, 0.8, 0.9, and 0.95, whose value is 0.8 or higher is *shaded*

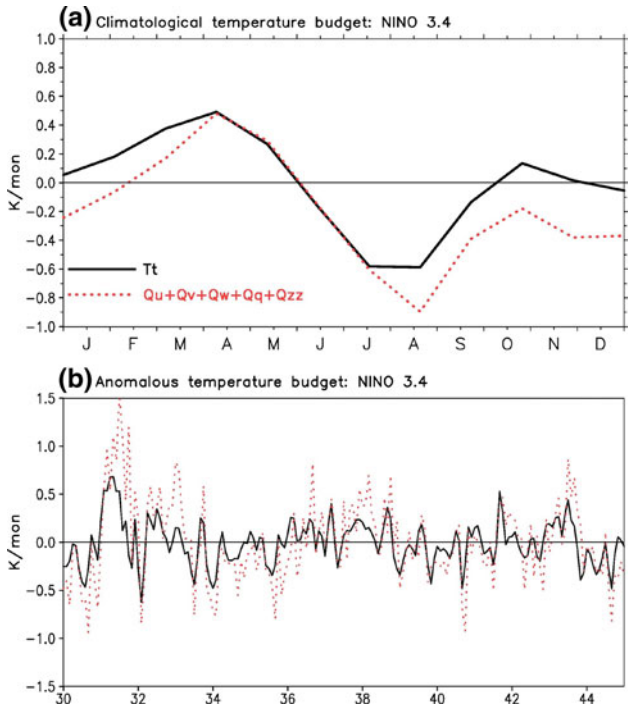

Fig. 12 Same as Fig. 3 except for temperature budget calculated using monthly averaged variables. The correlation coefficient between T_t and the forcing ($Q_u + Q_v + Q_w + Q_{zz} + Q_q$) is 0.92 and 0.74 in (**a**) and (**b**), respectively

More importantly, the climatological forcing ($Q_u + Q_v + Q_w + Q_q + Q_{zz}$) is systematically lower than T_t in the boreal fall and winter seasons when monthly outputs are used (Fig. 12a), while the agreement between T_t and forcing is much better when daily outputs are used (Fig. 3a). Similarly, the discrepancy between T_t and forcing in the interannual timescale is much larger by using monthly outputs (Fig. 12b) than by using daily outputs (Fig. 3b). Likewise, the forcing is systematically higher than T_t during the onset and development of the composite El Niño when monthly outputs are used (Fig. 13e), while the discrepancy is small when daily outputs are used (Fig. 7e). The discrepancy is partially associated with the unresolved damping effect from TIW when monthly outputs are used (Fig. 13b, c, d). By using monthly outputs, the difference between forcing and T_t may even be larger than T_t itself, e.g. between Jul and Dec of year 0 in Fig. 13e. The reason is that the zonal and meridional advection in Fig. 13a appear to have been overestimated during the El Niño development when they are compared with those in Fig. 7a. When daily outputs are used, the zonal advection is largely in phase with T_t, leading other advective terms by 2–4 months (Fig. 7a). However, the zonal advection lags T_t by 2 months when monthly outputs are used (Fig. 13a).

Our analyses suggest that high frequency variability (shorter than 30 days) in CFS makes significant contribution to advective terms, particularly the eddy term in zonal advection, and therefore it should be resolved in the heat budget analysis of ENSO. However, the large difference between heat budgets using daily and monthly averaged temperature and currents may be model dependent, and could be related to the model bias that CFS severely overestimates intraseasonal variability in the eastern Pacific (Wang et al. 2005).

6 Summary

The mixed layer heat budget for an 8-event composite of El Niño is diagnosed using 60-year daily outputs from the NCEP CFS. We find that ocean advection related to all components of oceanic currents plays an important role in the onset, development, decay, and phase transition of the El Niño in the tropical Pacific. A brief synthesis of the analysis is as follows:

(a) The major contributors to the onset, development, decay, and transition of the El Niño are the zonal advection induced by anomalous zonal current ($-u' \cdot \bar{T}_x$), vertical advection induced by mean upwelling ($-\bar{w} \cdot T'_z$), and meridional advection induced by both mean ($-\bar{v} \cdot T'_y$) and anomalous ($-v' \cdot \bar{T}_y$) meridional

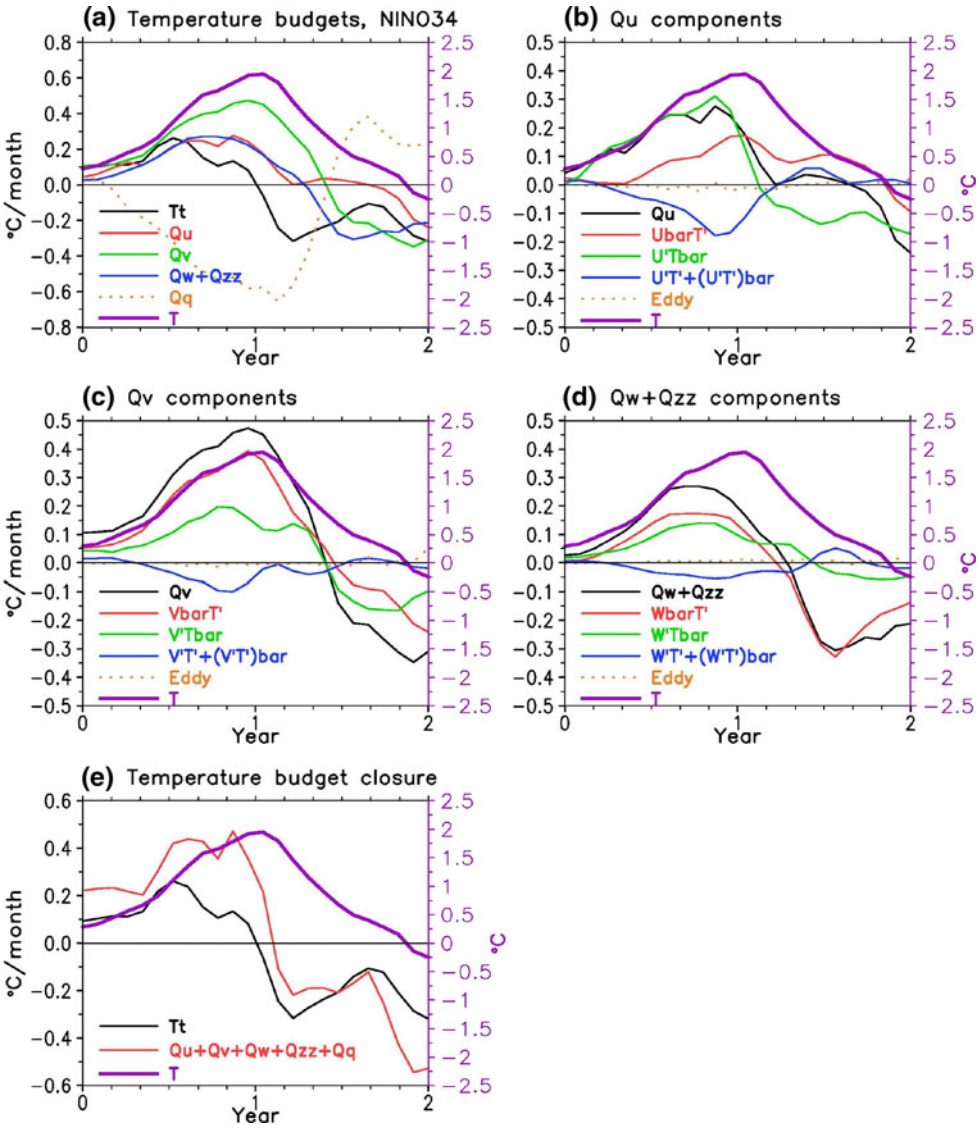

Fig. 13 **a–d** Same as Fig. 7 except for temperature budget anomalies calculated using monthly variables. **e** Temperature budget closure

current. Vertical advection by mean upwelling is narrowly confined in the equatorial Pacific, and is stronger in the eastern tropical Pacific. Meridional advection by mean and anomalous meridional current is almost equally important to the El Niño evolution; and their combined influence is larger than zonal advection or vertical advection.

(b) The zonal advection by mean zonal current $(-\bar{u} \cdot T_x')$ contributes to the El Niño development, but tends to maintain the El Niño during its decay phase. The vertical advection by anomalous vertical current $(-w' \cdot \bar{T}_z)$ contributes to the onset and development in the magnitude similar to the mean upwelling does, but its role is very limited in the transition phase.

(c) The role of all the non-linear terms is generally to damp the El Niño development. The role of the eddy is to weaken the El Niño development in longitudinal and latitudinal directions but to slightly strengthen the El Niño development in vertical direction.

(d) The seed for the phase transition of El Niño starts well before the peak phase, and is related to the cooling due to the vertical advection terms in the western Pacific. The initiation of the cooling seems to be associated with the upwelling in the western Pacific in the deeper ocean related to the mass divergence of downwelling surface water farther east (see Figs. 5g, 6e, 10). Along with the development of the El Niño, the cooling in the west also intensifies, moves eastward, and eventually leads to the decay of the El Niño.

(e) A higher temporal resolution such as daily or five-day averaged (Huang et al. 2010) outputs is needed to ensure the closure of diagnosed heat budget. The heat budget diagnosed from monthly outputs may

contaminate the heat budget closure, lower the correlation between forcing and temperature tendency, and therefore lower the reliability of the diagnosed mechanisms.

The role of anomalous zonal current and mean upwelling in the El Niño is known as the zonal advective and thermocline feedbacks in ENSO literature (Jin 1997; Jin and An 1999), and has been documented in coupled model simulations (An and Jin 2001; Zhang et al. 2007), ocean model simulations (Vialard et al. 2001), ocean reanalysis (Kim et al. 2007; Huang et al. 2010), and observations (Hayes et al. 1991; Kessler and McPhaden 1995; Frankignoul et al. 1996; Picaut et al. 1996; Wang and McPhaden 2000, 2001; Zhang and McPhaden 2006, 2008). Our analysis shows that both feedbacks are important for the El Niño onset, development, and decay; and that phase transition is well represented in the CFS.

Our analysis indicates that both mean and anomalous meridional current play an important role in the development, decay, and phase transition of El Niño, which is consistent with earlier ocean model simulations (Battisti 1988; Barnett and Latif 1991). Therefore, we can combine the effects of mean and anomalous currents into a single meridional advection feedback.

Analyses on the mixed layer heat budget of every individual El Niño event indicates that mechanisms of zonal, meridional, and upwelling feedbacks are robust as revealed in the composite El Niño, and can be used to compare with those in other models. The evolution of heat budget for individual El Niño may differ, however, from the El Niño composite (Fig. 7), due to large variations of 90–120 days in anomalous zonal currents (Fig. 5e) and zonal advection (Fig. 7b).

It has been noted that the evolutions of El Niño and La Niña are not symmetric (e.g. Su et al. 2010). We have also examined the heat budget for the composite La Niña. In our analysis, the damping effect of the surface heat flux in La Niña events is not as strong as in El Niño events. The nonlinear terms are weaker in La Niña events that in El Niño events. The variations of 90–120 days in La Niña events are not as active as in El Niño events. Despite these differences, the features of zonal, meridional, and upwelling feedbacks and damping effect from the TIW for the La Niña events are generally similar to those for the El Niño events.

References

Alexander MA, Matrosova L, Penland C, Scott JD, Chang P (2008) Forecasting Pacific SSTs: linear inverse model predictions of the PDO. J Clim 21:385–402

An S-I (2008) Interannual variations of the tropical ocean instability wave and ENSO. J Clim 21:3680–3686

An S-I, Jin F-F (2001) Collective role of thermocline and zonal advective feedbacks in the ENSO mode. J Clim 14:3421–3432

An S-I, Jin F-F (2004) Nonlinearity and asymmetry of ENSO. J Clim 17:2399–2412

Barnett TP, Latif M (1991) On ENSO physics. J Clim 4:487–515

Barnett TP, Dumenil L, Schlese U, Roeckner E (1988) The effect of Eurasian snow cover on global climate. Science 239:504–507. doi:10.1126/science.239.4839.504

Battisti DS (1988) Dynamics and thermodynamics of a warming event in a coupled tropical atmosphere-ocean model. J Atmos Sci 45:2889–2919

Battisti DS, Hirst AC (1989) Interannual variability in the tropical atmosphere/ocean system: influence of the basic state and ocean geometry. J Atmos Sci 46:1687–1712

Behera SK, Luo JJ, Masson S, Rao SA, Sakuma H, Yamagata T (2006) A CGCM study on the interaction between IOD and ENSO. J Clim 19:1688–1705

Behringer DW, Xue Y (2004) Evaluation of the global ocean data assimilation system at NCEP: the Pacific Ocean. Preprints, Eighth symposium on integrated observing and assimilation systems for atmosphere, oceans, and land surface, American Meterological Society, Seattle, WA, 2.3 [Available online at http://ams.confex.com/ams/84Annual/techprogram/paper_70720.htm.]

Bjerknes J (1969) Atmospheric teleconnections from the equatorial Pacific. Mon Wea Rev 97:163–172

Chang P, Saravanan R, Ji L (2003) Tropical atlantic seasonal predictability: the roles of El Niño remote influence and thermodynamic air-sea feedback. Geophys Res Lett 30. doi:10.1029/2002GL016119

Contreras RF (2002) Long-term observations of tropical instability waves. J Phys Oceanogr 32:2715–2722

Frankignoul C, Bonjean F, Reverdin G (1996) Interannual variability of surface currents in the tropical Pacific during 1987–1993. J Geophys Res 101:3629–3647

Galanti E, Tziperman E (2000) ENSO's phase locking to the seasonal cycle in the fast-SST, fast-wave, and mixed-mode regimes. J Atmos Sci 57:2936–2950

Gill AE (1980) Some simple solutions for heat induced tropical circulation. Quart J Roy Meteor Soc 106:1293–1302

Gray WM (1984) Atlantic seasonal hurricane frequency. Part I: El Niño and 30 mb Quasi-Biennial oscillation influences. Mon Wea Rev 112:1649–1668

Hayes SP, Chang P, McPhaden MJ (1991) Variability of the sea surface temperature in the eastern equatorial Pacific during 1986–1988. J Geophys Res 96:10533–10566

Hu Z-Z, Huang B (2007) The predictive skill and the most predictable pattern in the tropical Atlantic: the effect of ENSO. Mon Wea Rev 135:1786–1806

Huang B, Xue Y, Zhang D, Kumar A, McPhaden MJ (2010) The NCEP GODAS ocean analysis of the tropical Pacific mixed layer heat budget on seasonal to interannual time scales. J Clim 23:4901–4925

Jin F-F (1997) An equatorial ocean recharge paradigm for ENSO. Part I: conceptual model. J Atmos Sci 54:811–829

Jin F-F, An S-I (1999) Thermocline and zonal advection feedbacks within the equatorial ocean recharge oscillator model for ENSO. Geophys Res Lett 26:2989–2992

Jin F-F, An S-I, Timmermann A, Zhao J (2003) Strong El Niño events and nonlinear dynamical heating. Geophys Res Lett 30: 1120. doi:10.1029/2002GL016356

Jin EK, Kinter JL, Wang B, Park C-K, Kang I-S, Kirtman BP, Kug J-S, Kumar A, Luo J-J, Schemm J (2008) Current status of ENSO prediction skill in coupled ocean–atmosphere models. Clim Dyn 31:647–664. doi:10.1007/s00382-008-0397-3

Jochum M, Murtugudde R (2006) Temperature advection by tropical instability waves. J Phys Oceanogr 36:592–605
Kang I-S, An S-I, Jin F-F (2001) A systematic approximation of the SST anomaly equation for ENSO. J Meteor Soc Japan 79:1–10
Kessler WS, McPhaden MJ (1995) The 1991–93 El Niño in the central Pacific. Deep-Sea Res 42:295–333
Kessler WS, McPhaden MJ, Weickmann KM (1995) Forcing of intraseasonal Kelvin waves in the equatorial Pacific. J Geophys Res 100:10613–10631. doi:10.1029/95JC00382
Kessler WS, Rothstein LM, Chen D (1998) The annual cycle of SST in the eastern tropical Pacific, diagnosed in an ocean GCM. J Clim 11:777–799
Kim S-B, Lee T, Fukumori I (2007) Mechanisms controlling the interannual variation of mixed layer temperature averaged over the Niña-3 region. J Clim 20:3822–3843
Large WG, McWilliams JC, Doney SC (1994) Oceanic vertical mixing: a review and a model with nonlocal boundary layer parameterization. Rev Geophys 32:363–403
Latif M, Anderson D, Barnett T, Cane M, Kleeman R, Leetmaa A, O'Brien J, Rosati A, Schneider E (1998) A review of the predictability and prediction of ENSO. J Geophys Res 103:14375–14393
McPhaden MJ, Hayus SP, Mangum LJ, Toole JM (1990) Variability in the western equatorial pacific ocean during the 1986–87 El Niño/southern oscillation event. J Phys Oceanogr 20:190–208
Meinen CS, McPhaden MJ (2000) Observations of warm water volume changes in the equatorial Pacific and their relationship to El Niño and La Niña. J Clim 13:3551–3559
Menkes CE, Vialard JG, Kennan SC, Boulanger JP, Madec GV (2006) A modeling study of the impact of tropical instability waves on the heat budget of the eastern equatorial Pacific. J Phys Oceanogr 36:847–865
Mokhov II, Smirnov DA (2006) El Niño–southern oscillation drives north Atlantic oscillation as revealed with nonlinear techniques from climatic indices. Geophys Res Lett 33:L03708. doi:10.1029/2005GL024557
Newman M, Compo GP, Alexander MA (2003) ENSO-forced variability of the pacific decadal oscillation. J Clim 16:3853–3857
Pacanowski RC, Griffies SM (1999) MOM 3.0 manual. NOAA/Geophysical Fluid Dynamics Laboratory, Princeton, New Jersey, 668 pp
Pegion K, Kirtman BP (2008) The impact of air-sea interactions on the simulation of tropical intraseasonal variability. J Clim 21:6616–6635
Philander SG (1990) El Niño, La Niña, and the southern oscillation. Academic Press, London, p 293
Picaut J, Ioualalen M, Menkes C, Delcroix T, McPhaden MJ (1996) Mechanism of the zonal displacements of the pacific warm pool: implications for ENSO. Science 29. doi:10.1126/science.274.5292.1486
Rasmusson EM, Carpenter TH (1982) Variations in tropical sea surface temperature and surface wind fields associated with the southern oscillation/El Niño. Mon Wea Rev 110:354–384
Ropelewski CF, Halpert MS (1986) North American precipitation and temperature patterns associated with the El Niño/southern oscillation (ENSO). Mon Wea Rev 114:2352–2362
Saha S, Nadiga S, Thiaw C, Wang J, Wang W, Zhang Q, van den Dool HM, Pan H-L, Moorthi S, Behringer D, Stokes D, White G, Lord S, Ebisuzaki W, Peng P, Xie P (2006) The NCEP climate forecast system. J Clim 19:3483–3517
Schopf PS, Suarez MJ (1988) Vacillations in a coupled ocean-atmosphere model. J Atmos Sci 45:549–568
Seo K-H, Xue Y (2005) MJO-related oceanic Kelvin waves and the ENSO cycle: a study with the NCEP global ocean data assimilation system. Geophys Res Lett 32:L07712. doi:10.1029/2005GL022511
Sprintall J, Tomczak M (1992) Evidence of the barrier layer in the surface layer of the tropics. J Geophys Res 97:7305–7316
Su J, Zhang R, Li T, Rong X, Kug J-S, Hong C-C (2010) Causes of the El Niño and La Niña amplitude asymmetry in the equatorial eastern Pacific. J Clim 23:605–617
Suarez MJ, Schopf PS (1988) A delayed action oscillator for ENSO. J Atmos Sci 45:3283–3287
Tziperman E, Cane MA, Zebiak SE, Xue Y, Blumenthal B (1998) Locking of El Nino's peak time to the end of the calendar year in the delayed oscillator picture of ENSO. J Clim 11:2191–2199
Vialard J, Menkes C, Boulanger J-P, Delecluse P, Guilyardi E, McPhaden MJ, Madec G (2001) A model study of oceanic mechanisms affecting equatorial Pacific sea surface temperature during 1997–1998 El Nino. J Phys Oceanogr 31:1649–1675
Wang W, McPhaden MJ (2000) The surface-layer heat balance in the equatorial pacific ocean. Part II: interannual variability. J Phys Oceanogr 30:2989–3008
Wang W, McPhaden MJ (2001) Surface layer temperature balance in the equatorial Pacific during the 1997–1998 El Nino and 1998–1999 La Nina. J Clim 14:3393–3407
Wang B, Wu R, Fu X (2000) Pacific–East Asian teleconnection: how does ENSO affect East Asian climate? J Clim 13:1517–1536
Wang W, Saha S, Pan H-L, Nadiga S, White G (2005) Simulation of ENSO in the New NCEP coupled forecast system model (CFS03). Mon Wea Rev 133:1574–1593
Webster PJ, Magana VO, Palmer TN, Tomas TA, Yanai M, Yasunari T (1998) Monsoons: processes, predictability, and prospects for prediction. J Geophys Res 103:14451–14510
Wrytki K (1975) El Niño-The dynamic response of equatorial Pacific Ocean to atmospheric forcing. J Phys Oceanogr 5:572–584
You Y (1995) Salinity variability and its role in the barrier-layer formation during TOGA-COARE. J Phys Oceanogr 25:2778–2807
Yu J-Y, Liu WT (2003) A linear relationship between ENSO intensity and tropical instability wave activity in the eastern Pacific Ocean. Geophys Res Lett 30. doi:10.1029/2003GL017176
Yu J-Y, Mechoso CR (2001) A coupled atmosphere-ocean GCM study of the ENSO cycle. J Clim 14:2329–2350
Yulaeva E, Wallace JM (1994) The signature of ENSO in global temperature and precipitation fields derived from the microwave sounding unit. J Clim 7:1719–1736
Zebiak SE, Cane MA (1987) A model El Niño-southern oscillation. Mon Wea Rev 115:2262–2278
Zhang X, McPhaden MJ (2006) Wind stress variations and interannual sea surface temperature anomalies in the eastern equatorial Pacific. J Clim 19:226–241
Zhang X, McPhaden MJ (2008) Eastern equatorial Pacific forcing of ENSO sea surface temperature anomalies. J Clim 21:6070–6079
Zhang X, McPhaden MJ (2010) Surface layer heat balance in the eastern equatorial Pacific Ocean on interannual time scales: influence of local versus remote wind forcing. J Clim 23:4375–4394
Zhang Q, Kumar A, Xue Y, Wang W, Jin F-F (2007) Analysis of the ENSO cycle in the NCEP coupled forecast model. J Clim 20:1265–1284